LITHOS 516–517 (2025) 108265

Contents lists available at ScienceDirect

LITHOS

journal homepage: www.elsevier.com/locate/lithos

Mineralogy and provenance of the Chang'e-6 shoveled lunar samples

Shanna Xue [a], Wenlei Song [a,*], Zhuang Guo [a,*], Yuqi Qian [b], Kangjun Huang [a], Chao Zhang [a], Qian Liu [a], Xiaojun Wang [a], Le Qiao [a], Qian Chen [a], Donghai Zhang [a], Lihui Chen [a], Honglin Yuan [a], Guochun Zhao [a,b]

[a] State Key Laboratory of Continental Evolution and Early Life & NWU-HKU Joint Center of Earth and Planetary Sciences, Department of Geology, Northwest University, Xi'an 710069, China
[b] NWU-HKU Joint Center of Earth and Planetary Sciences, Department of Earth Sciences, The University of Hong Kong, Hong Kong, China

ARTICLE INFO

Keywords:
Chang'e-6
Lunar soil
Statistical mineralogy
Provenance composition

ABSTRACT

Lunar regolith develops through continuous gardening resulting from various space weathering processes. The Chang'e-6 (CE-6) mission landed on the lunar farside within the geologically complex South Pole-Aitken basin that was modified by impact events. Soil collected from this site preserves a detailed record of lunar geological evolution. The fine-grained regoliths reflect extensive mechanical fragmentation and mixing, and they closely match the landing area's average mineralogy. This study provides a statistical evaluation of the mineralogy, bulk geochemistry, and provenance of the CE-6 fine-grained soils (70,437 particles) using automated quantitative mineralogy and mineral chemistry analysis. The examined particles, mostly ≤30 μm in size, comprise approximately 93.5 vol% of mare basalts (plagioclase: 27.5 %; glass: 32.3 %; pyroxene: 28.2 %; olivine: 0.7 %; ilmenite: 1.9 %; Si-rich phase: 1.2 %) and approximately 6.5 vol% of exotic non-mare components. Exotic components consist mainly of anorthite (An ≥ 95) and pyroxene (En < 50) from ferroan anorthosite (FAN) (0.9 %; 0.3 %), low-Ca pyroxene (Wo ≤ 5, 1.2 %, norite), Mg-rich pyroxene (En ≥ 50, 1.3 %), equivalent plagioclase from Mg-suite clast (~2.5 %) and magnesian olivine from the troctolite and mantle materials (Fa ≤ 20, 0.3 %). Compared to Chang'e-5 basalts, the CE-6 samples show higher glass abundance and elevated Al_2O_3, CaO, and $Mg^{\#}$, but lower FeO levels. These differences suggest a longer history of impact gardening with more exotic non-mare components at the CE-6 sampling site. This study provides the first direct and statistically robust mineralogical evidence constraining the provenance of CE-6 soils, supporting and refining previous interpretations of lunar regolith evolution.

1. Introduction

Lunar soil is a long-term space weathering product of lunar rocks, which are constantly broken, mixed, melted, re-broken, and re-cemented. It is primarily composed of rock fragments, mineral grains, breccias, impact glass, and agglutinates (Heiken et al., 1991; Lucey, 2006). The composition of lunar soil provides important information about the formation and evolution of the lunar surface, particularly in terms of its mineralogical and chemical signatures that can be traced to their provenance. Specifically, the presence of exotic materials in lunar soils provides critical evidence for reconstructing the lunar impact and geological history.

Current estimates of exotic mineralogical composition in lunar soils are largely based on impact ejecta and regolith overturning modeling (Sharpton, 2014; Su et al., 2024; Xu et al., 2021) and bulk chemical compositions (Zong et al., 2022), which have been widely applied to the Chang'e-5 (Jia et al., 2022; Qian et al., 2021) and Chang'e-6 sampling site (Xu et al., 2024; Zhang et al., 2025) investigations. This approach often lacks limited petrological and mineralogical validation from returned samples, which introduces potential uncertainties in estimating the proportion of exotic materials in lunar soils. For example, in the regolith sourced from within the CE-5 basalt unit (Em4/P58 unit, Hiesinger et al., 2011), numerical modeling calculations and remote-sensing observations indicate that approximately >10–20 % of the

* Corresponding authors.
E-mail addresses: xueshanna@stumail.nwu.edu.cn (S. Xue), wlsong@nwu.edu.cn (W. Song), guozhuang@nwu.edu.cn (Z. Guo), yuqiqian@hku.hk (Y. Qian), hkj@nwu.edu.cn (K. Huang), zhangchao@nwu.edu.cn (C. Zhang), liuqian@nwu.edu.cn (Q. Liu), wangxj@nwu.edu.cn (X. Wang), 202421988@stumail.nwu.edu.cn (L. Qiao), 201921080@stumail.nwu.edu.cn (Q. Chen), dhzhang@nwu.edu.cn (D. Zhang), chenlh@nwu.edu.cn (L. Chen), hlyuan@nwu.edu.cn (H. Yuan), gczhao@icloud.com (G. Zhao).

https://doi.org/10.1016/j.lithos.2025.108265
Received 3 July 2025; Received in revised form 18 September 2025; Accepted 18 September 2025
Available online 23 September 2025

materials originate from outside this unit (Jia et al., 2022; Qian et al., 2021; Xie et al., 2020). However, laboratory analyses of CE-5 samples revealed significantly lower proportions of exotic materials (< 5 %) (Chen et al., 2023; Zeng et al., 2022; Zong et al., 2022). This discrepancy highlights the importance of conducting direct and comprehensive mineralogical and statistical analyses to constrain the evolutionary history and accurately estimate the proportion of exotic materials in lunar soil.

Previous studies have demonstrated that lunar soil fractions smaller than <45 μm most closely resemble bulk soil composition (Cao et al., 2022; Fischer, 1995; Pieters et al., 1993). Therefore, detailed, comprehensive, and systematic mineralogical and geochemical work on fine-grained lunar soils is important for understanding the provenance of lunar soils and interactions between the lunar surface and the space environment. However, investigating and reconstructing the mineralogy and evolution of the underlying bedrock using fine-grained lunar soil is exceedingly challenging, because the soil samples are characterized by not only micron-scale small sizes, but also diverse mineral assemblages, textures, and compositions from particle to particle. Traditional analytical methods (e.g., SEM-EDS, EPMA, LA-ICP-MS) are highly time-consuming and unsuitable for high-throughput statistical analysis of hundreds of thousands of particles in lunar soils. The automated mineralogy systems, which have been widely used in optimizing process mineralogy for ore slags and powders (e.g., Beinlich et al., 2020; Breiter et al., 2018; Xu et al., 2018, 2017), have been recently successfully applied in providing rapid, quantitative, and reliable mineralogical and compositional data for CE-5 lunar soils (Chen et al., 2024).

The CE-6 mission successfully returned 1935.3 g of samples for the first time from the farside of the Moon, in the deepest and oldest basin (SPA) on the Moon (Li et al., 2024). Recent research suggests that volcanic activity on the lunar farside began before 2.8 Ga (Cui et al., 2024; Zhang et al., 2024b). The CE-6 landing site had a complex impact history, with the collected lunar soils coming from a mix of materials (Melosh et al., 2017; Potter et al., 2018; Yue et al., 2024). Impact gardening process models suggest that the CE-6 lunar soil sampled from the top ~1 m deep layer mainly comprises intermediate-Ti basalts and a minor fraction of exotic materials (~9.3 %) derived from the surrounding impact crater (e.g., Chaffee S, Vavilov, Crookes, and Das) (Su et al., 2024; Xu et al., 2024). These models further suggest that the CE-6 lunar soil contains 6.1 % SPA basin materials and 0.6 % highland feldspathic materials, likely representing components from the mantle and crust, respectively (Zhang et al., 2025). However, direct mineralogical and geochemical evidence from returned CE-6 samples to support these models is limited.

To accurately constrain the provenance of the CE-6 landing site using lunar soil samples, the automated quantitative mineralogy (TESCAN integrated mineral analyzer, TIMA) in combination with EPMA and LA-ICPMS were used to analyze and quantitatively characterize the morphology, mineralogy, and bulk chemical composition of CE-6 fine-grained lunar soil. The results provide direct, statistically significant mineralogical evidence regarding the abundance and composition of mare basalts and exotic non-mare components in the CE-6 sample. These findings offer an ideal reference framework for understanding the provenance of the CE-6 landing site and contribute to broader interpretations of lunar geological evolution.

2. Sample and methods

This study used the scooped CE-6 lunar soil samples (CE6C0500YJFM), which were provided by the China National Space Administration. The soil particles were first dispersed and attached to the tape at the bottom of the mold, ensuring the formation of a single layer. Resin gel was injected, immersing all the particles. The resin cured quickly, and all the particles remained in contact with the surface of the resin. The mounts were polished and coated with carbon before analysis.

2.1. Automated quantitative mineralogy

The automated mineralogy investigation was conducted using a TESCAN Integrated Mineral Analyzer (TIMA) system at the State Key Laboratory of Continental Evolution and Early Life, Department of Geology, Northwest University, China. The system comprises a TESCAN MIRA-3 scanning electron microscopy (SEM) equipped with four EDAX Element 30 Energy Dispersive X-Ray Spectrum (EDS) detectors, combining advanced computer graphics and statistical techniques, and assisted by continuously updated professional mineral processing software. The system is designed to automatically identify and quantify minerals based on the combination of backscattered electron (BSE) signal intensity and characteristic X-rays generated during the electron beam-sample interaction, with high resolution ranging from microns to sub-microns.

The TIMA high-resolution mapping X-ray scanning acquisition mode with a BSE pixel and EDS spacing of 2 μm was used to obtain high-quality elemental compositional data for individual mineral grains, which serves as the basis for precise mineral classification. This mode features data processing capabilities that enable access to EDS composition and spectra, enabling systematic characterization of chemical variability within entire specific mineral populations, allowing for further subdivision of the category. The BSE image and EDS signal are obtained simultaneously across a predefined grid, point by point, for the set pixel area. Each EDS measurement point collects 20,000 X-ray counts to obtain high-quality compositional data, with full coverage of the analyzed area to identify all mineral phases comprehensively. Using a built-in automation program, the beam and BSE signal strengths are calibrated on the Faraday cup and platinum standards (Hrstka et al., 2018). The measurements were conducted at a beam current of 9 nA, an acceleration voltage of 25 kV, and a working distance of 15 mm. For more methodological details, refer to Chen et al., 2024.

A total of 100,419 lunar soil particles were analyzed within 40 h, of which 29,982 particles were < 2 μm. Due to the relatively large electron beam interaction volume (typically 2–3 μm), which can produce the mixed spectral signals from adjacent phases in fine-grained minerals (Graham and Keulen, 2019), particles below 2 μm size threshold were excluded from quantitative mineralogical analysis to ensure spectral reliability. Therefore, 70,437 lunar soil particles larger than 2 μm were selected for quantitative studies. For each identified phase, the average chemical composition was determined by summarizing multiple measurement points using the TIMA "*Spectrum tool*". These computed chemical compositions and their corresponding EDS spectra served as reference components to define each mineral phase. The identification and classification were further validated by EPMA analysis, which confirmed consistency with the TIMA EDS elemental spectral lines and compositions. Based on well-documented differences in mineral chemistries among various lunar rock types (e.g., Heiken et al., 1991), classification rules for mare basaltic and exotic non-mare components were established within the TIMA system (Table S1, see Supplementary Text S1 for details). These rules are based on the peak intensities of each elemental line acquired from the tested spectrum. The ranges for the selected rules of a certain mineral are based on its spectral signature with an adjustable confidence value. The TIMA software (version 2.11.0) filtered and matched all analyzed minerals against a mineral library previously established for CE-5 samples (Chen et al., 2024), classifying and quantifying particles whose compositions fell within the defined ranges. The TIMA software enabled the systematic determination of mineralogical classification, modal abundance, chemical composition, and particle size for the CE-6 lunar soil particles, ultimately yielding the provenance proportions of the fine-grained fraction.

2.2. Major component analysis

Major element compositions of plagioclase, pyroxene, olivine, and ilmenite in CE-6 lunar soils (Table S2) were analyzed using a JEOL JXA-

IPH200F field-emission electron probe microanalyzer at the State Key Laboratory of Continental Evolution and Early Life, Northwest University, China. Point analyses were performed on all the mineral grains using an accelerating voltage of 15 kV. To optimize analytical precision and minimize volatilization, beam conditions were tailored for each mineral: Plagioclase was analyzed using a 2-μm-diameter electron beam with a 10-nA current. Olivine and pyroxene were analyzed using a 1 μm diameter electron beam with 15 nA. Ilmenite was analyzed using an electron beam with a diameter of 1 μm and a current of 20 nA. The background counting time was set to 1/2 of the peak counting time, measured on both high- and low-energy background positions. The following well-characterized reference materials were used for elemental concentration calibration: Plagioclase: Orthoclase (K), Rutile (Ti), Albite (Si, Na), Olivine (Mg), Diopside (Ca), Almandine (Fe), Rhodonite (Mn), Albite (Na), Pyrope (Al); Pyroxene and Olivine: Diopside (Ca), Rutile (Ti), Olivine (Si, Mg), NiO (Ni), Cr_3O_2 (Cr), Almandine (Fe), Rhodonite (Mn), Pyrope (Al); Ilmenite: Rutile (Ti), Orthoclase (K), Diopside (Ca), Olivine (Si, Mg), Hf (Hf), Almandine (Fe), Rhodonite (Mn), Co (Co), Cr_3O_2 (Cr), V (V), NiO (Ni), Albite (Na), Pyrope (Al), Ta (Ta). For wavelength dispersive X-ray spectroscopy (WDS), the following diffraction crystals were used: TAPL (Na, Mg, Al, Si), PET (K, Ca), LIFH (Fe, Mn, Co, Ti), and LIFL (Cr, V, Ta). All acquired data were reduced and corrected using the ZAF procedure.

2.3. Trace element measurement

Trace element compositions analysis of major minerals (Table S3) were determined using a Thermo Scientific iCap TQ inductively coupled plasma mass spectrometry (Q-ICPMS) coupled with an ASI Resolution LR 193 nm ArF excimer laser ablation (LA) system. The LA system utilized helium (He) carrier gas at a flow rate of 350 mL/min, and the 0.95 L/min flow nebulizer argon (Ar) gas, supplied by the iCap TQ, was introduced into the funnel to mix with He carrier prior to entering the ICP torch. Standards and samples were analyzed using a laser diameter of 9 μm, repetition rate of 8 Hz, and energy output density of 3 J/cm^2. Each analysis cycle consisted of 3-plus surface cleanings, 7 s washout, 15 s background, 20 s of sample ablation, and 5 s washout. USGS reference glasses (BCR-2G, BIR-1G, and BHVO-2G) and NIST glasses (SRM610 and SRM612) were analyzed as external standards. The contents of Si (for silicate minerals) and Fe (for ilmenite) obtained by EPMA were used as internal standards and corrected by Iolite 4 software (Paton et al., 2011).

2.4. Major element calibration for TIMA

The bulk chemical composition of the soils (Table S4) was calculated based on the modal abundance of constituent minerals and their average elemental compositions. The mineral compositions in the mineral classification library for calculation can be directly obtained from the TIMA-collected EDS spectrum or manually input based on the relevant high-precision external analysis (e.g., EPMA). These external analyses are particularly important for minerals containing elements near or below the detection limit of the EDS system (Hrstka et al., 2018). As the TIMA software calculates bulk composition based on elemental weight percentages (wt%), all oxide-based EPMA data were converted to their elemental equivalents prior to input. The conversion was performed using the formula:

$$X = Y^{*}\frac{Ar^{*}Z}{Mr} \quad (1)$$

where X is elemental weight percentage (wt%); Y is oxide weight percentage (wt%); Z is cation number; Ar is the relative atomic mass; Mr. is the relative molecular mass; e.g., the elemental Si weight percentage from SiO_2 is calculated as: $Si = SiO_2{}^{*}(28.09/(28.09 + 15.99{*}2))$. These calculated values were manually assigned to the mineral composition of the TIMA library, and the software integrated these values and measured mineral modal abundances to calculate the corresponding bulk chemical composition of the soil samples.

3. Results

3.1. Mineralogy of CE-6 fine-grained lunar soils

The particle size of the sample (70,437 particles) ranges from 2 to 80 μm, with ~97.9 % ≤30 μm ($n = 68,951$) and ~ 0.11 % >50 μm ($n = 80$) (Fig. 1a). Quantitative mineralogical analysis (Table S5) shows that the minerals of CE-6 fine-grained lunar soil consists of plagioclase (31.0 vol %), glass (32.3 vol%), augite (20.4 vol%), pigeonite (9.4 vol%), orthopyroxene (1.2 vol%) and ilmenite (1.9 vol%), with small amount of olivine (fayalite, 0.4 vol%; forsterite, 0.6 vol%), Si-rich phases (1.2 vol %), troilite (0.1 vol%) and minor unidentified minerals (1.6 vol%) (Fig. 1b-j, Table S5), which is consistent with the reported results obtained by X-ray diffraction analyzer (XRD) (Sample: CE6C0000YJFM, plagioclase: 32.6 %, amorphous glass: 29.4 %, augite: 19.7 %, pigeonite: 10 %, orthopyroxene: 3.6 %, olivine: 0.5 %. Li et al., 2024). The pyroxene compositions (Table S2) are variable, mostly composed of augite ($Wo_{24.4}En_{45.6}Fs_{30}$ on average, $n = 4$) and pigeonite ($Wo_{19.1}En_{27.8}Fs_{53}$ on average, $n = 3$, EPMA), except for a trace amount of orthopyroxene ($Wo_{2.9}En_{71.2}Fs_{25.9}$ on average, $n = 5$, EPMA, noritic material). All pyroxenes (Table S3) analyzed by LA-ICPMS have a broad range of REE abundance ($2.02 \times CI < REE < 535 \times CI$; CI: abundances of CI chondrite; Anders and Grevesse, 1989), which is generally lower than the CE-5 basalt (Tian et al., 2021, 2023). All three pyroxenes display LREE depletion ($0.05\times - 136\times$ CI) and deep negative Eu anomaly characteristics (Table S3), aligning with the reported CE-6 pyroxenes (Shen et al., 2025; Yin et al., 2025). The plagioclase is largely anorthite (~85 %), with an average composition of $An_{96.1}Ab_{3.7}Or_{0.2}$ ($n = 7$, EPMA, Table S2). In contrast to pyroxene, plagioclase is rich in LREE (~$19.23 \times$ CI) relative to HREE (most of which are below the detection limits) with a significant negative Eu anomaly (Table S3). Moreover, the analyzed plagioclase exhibits high abundances of Sr (129–630 ppm) and Ba (11.8–82.1 ppm), with the contents of La and Sr increasing gradually as the An content decreases (Table S3). The clasts in the fine-grained lunar soils are generally composed of a pyroxene-plagioclase-ilmenite assemblage (Fig. 1d-j), suggesting that the CE-6 shoveled sample mainly comprises mare basaltic fragments. The olivine (Table S2) consists mainly of forsterite ($Fo_{91–95}$; Fo = molar Mg/(Mg + Fe)*100) (n = 5, EPMA) and fayalite ($Fo_{22–29}$) ($n = 9$, EPMA).

Glass is excluded from provenance assessment for the following reasons. The glasses can be classified as agglutinate (Fig. S1a-b) and homogeneous spherical glass (Fig. S1c-d). Previous studies have shown that the local melting of basaltic fragments most likely formed agglutinate glasses, which are dominated by plagioclase with high Al_2O_3 and low MgO contents (Fig. S1e-f) (Ding et al., 2025; Long et al., 2022; Yang et al., 2022). The majority of the glass analyzed from agglutinates is not representative of exotic sources. Although homogeneous spherical glass (e.g., glass beads) exhibits compositional similarities to exotic components, recent studies show that small impact beads (<100 μm) with significant compositional deviations may not necessarily be exotic or have an extremely low proportion (Wang et al., 2025b). Therefore, we exclude the glass from the provenance analysis. The provenance results shows that the CE-6 fine-grained lunar soil is composed of at least ~93.5 vol% of mare basalts and ~ 6.5 vol% of exotic non-mare components (Fig. 1k, Fig. S2, Table 1), in which exotic components include plagioclase (ferroan anorthosite, FAN: 0.9 vol%; Mg-suite clast: 2.5 vol%), pyroxene (FAN: 0.3 vol%; norite: 1.2 vol%; other Mg-suite rocks: 1.3 vol %) and magnesian olivine (dunite and troctolite: 0.3 vol%) (Refer to Supplementary Text S1 for detailed classification of exotic non-mare components). Among them, the plagioclase in the Mg-suite exhibits a wide range of An values, which overlaps with the range of mare basalt (Heiken et al., 1991). Its abundance value is estimated using a 1:1 ratio

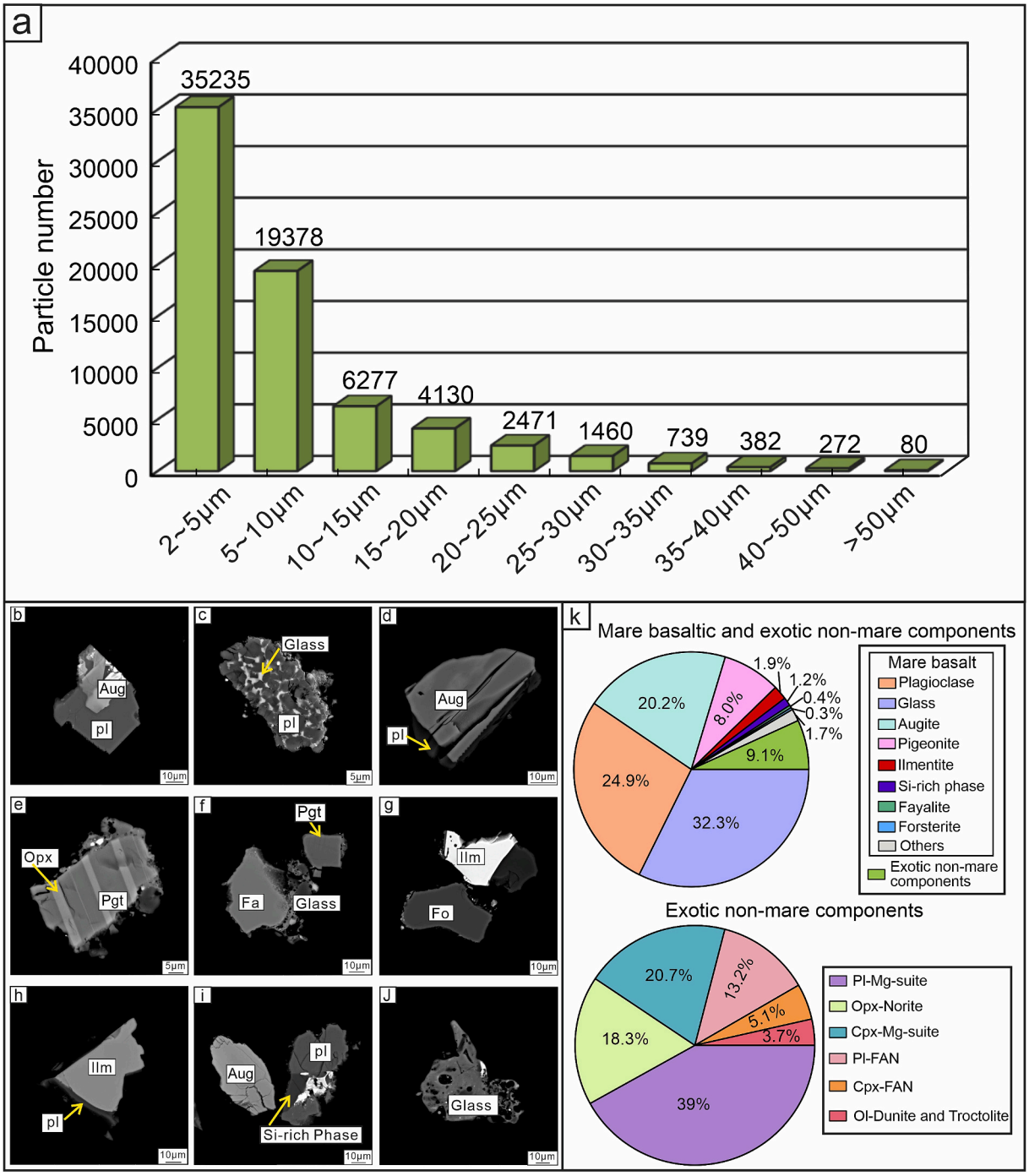

Fig. 1. Particle size and mineralogic characteristics of the CE-6 fine-grained lunar soils. (a) Histogram of particle size distribution; (b-j) The BSE images of some represent mineral particles (b-c, plagioclase; d, augite; e, pigeonite; f, fayalite; g, forsterite; h, ilmenite; i, Si-rich phase; j, glass); (k) Mineral modal abundance (vol%) analyzed by TIMA and the provenance of mare basaltic and exotic non-mare components. Abbreviation: Pl, Plagioclase; Aug, augite; Pgt, pigeonite; Fa, fayalite; Fo, forsterite; Ilm, Ilmenite; FAN, ferroan anorthosite.

of plagioclase to pyroxene in the Mg-suite (Sheng et al., 2025; Su et al., 2025). As the particle size decreases from 80 μm to 2 μm, the abundance of mare basalts increases, which is characterized by that plagioclase and glass increases (22.8–23.8 vol%; 19.6–56.6 vol%, respectively), the clinopyroxene were significantly reduced (Aug: 35.5–9.3 vol%; Pgt: 11.8–2.5 vol%) (Fig. 2, Table S6). However, the abundance of exotic non-mare components decreases with the decrease of particle size (Fig. 2, Table S6), which is demonstrated by the consistent reduction in the clinopyroxene population from FAN and Mg-suite clast (2.1–0.5 vol %), orthopyroxene from norite (2.2–1.6 vol%) and the slow decline of olivine from dunite and troctolite, and the slight increase of plagioclase from FAN (1.2–0.1 vol%).

3.2. Bulk chemical composition of CE-6 fine-grained lunar soils

The bulk chemical composition of the soils was calculated using the average elemental content (calibrated by EPMA) of the minerals and the mass fraction of the corresponding minerals in the soil particles. The major element composition after calibration is: SiO_2 (45.24 wt%), Al_2O_3 (17.60 wt%), FeO (14.15 wt%), MgO (6.63 wt%), CaO (12.72 wt%),

Table 1
The mare basaltic and exotic non-mare components abundances of CE-6 fine-grained lunar soils.

Minerals		vol%	wt%	Minerals		vol%	wt%
Mare basalts	Glass	32.3	31.3	Exotic non-mare components	Opx-Norite	1.2	1.2
	Plagioclase	27.5	26.6		Cpx-Mg-suite	1.3	1.3
	Augite	20.2	20.2		Cpx-FAN	0.3	0.3
	Pigeonite	8.0	8.1		Pl-FAN	0.9	0.8
	Ilmenite	1.9	3.4		Pl-Mg-suite[a]	2.5	2.6
	Si-rich phase	1.2	1.1		Ol-Dunite and Troctolite	0.3	0.4
	Fayalite	0.4	0.5				
	Forsterite	0.3	0.4				
	Others	1.7	1.8				
	Total	93.5	93.4		Total	6.5	6.6

FAN, ferroan anorthosite; Opx-Norite, Orthopyroxene-Norite; Cpx-Mg-suite, Clinopyroxene-Mg-suite.
[a] Based on the ratio 1:1 plagioclase to pyroxene in the norite and other Mg-suite (e.g., troctolite), the abundance of Pl-Mg-suite is the total of Cpx-Mg-suite and Opx-Norite.

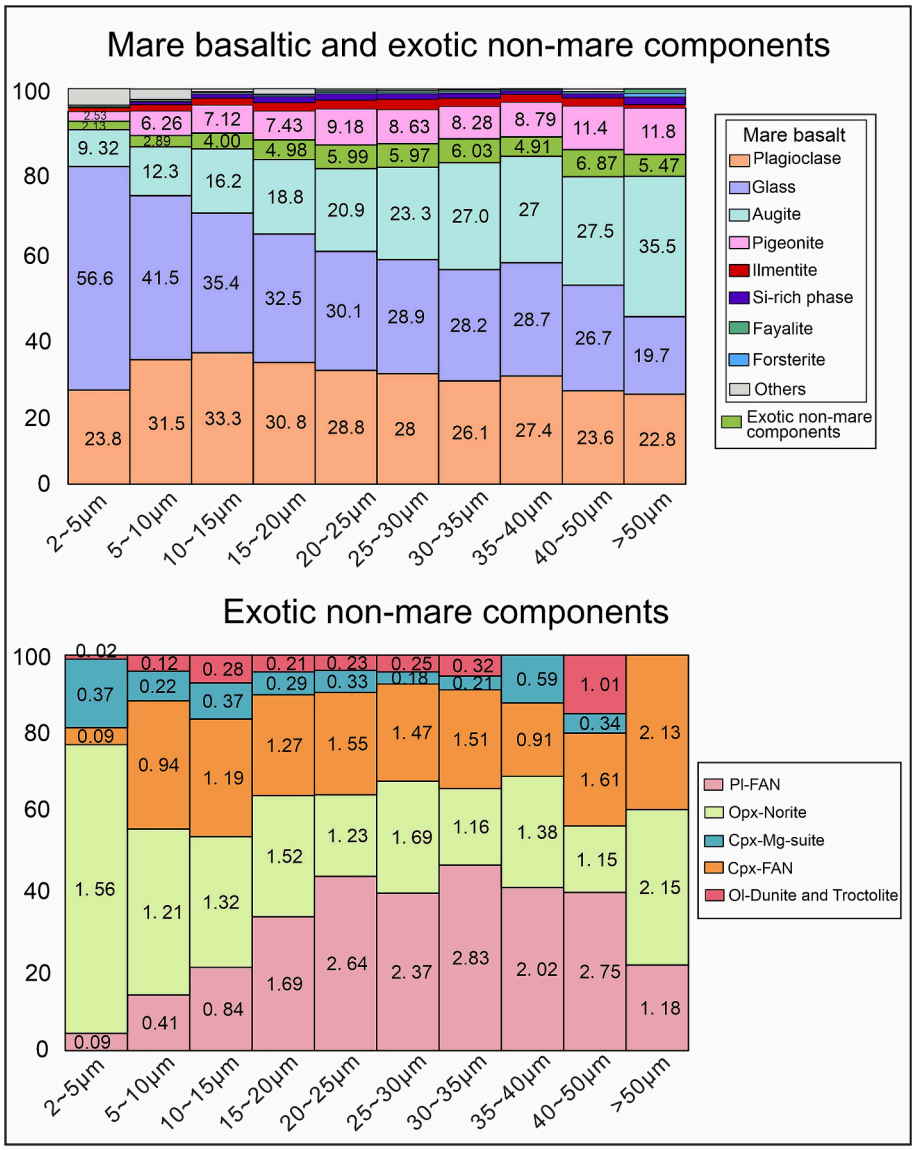

Fig. 2. Size-dependent mineral abundance of mare basaltic and exotic non-mare components (vol%) from the CE-6 fine-grained soils.

TiO_2 (2.17 wt%), Na_2O (0.24 wt%), K_2O (0.02 wt%), and $Mg^{\#}$ (45.52, molar Mg/(Mg + Fe)*100). Compared to the reported compositions of CE-6 soil and basalt samples analyzed by X-ray fluorescence spectrometry (XRF) (Table S4, Li et al., 2024; Yin et al., 2025), the CE-6 fine-grained samples exhibit higher Al_2O_3 and CaO concentration and lower FeO levels, which aligns with the mineral modal abundance, indicating variable mineral fragmentation within fine-grained lunar soils varies, with a higher proportion of plagioclase and glass and a lower proportion of pyroxene and ilmenite. The higher Mg/Fe values represent the mixing of exotic non-mare components (e.g., Mg-rich pyroxene from the Mg-

suite). In addition, the variation of bulk chemical composition varied significantly with the size of the fine-grained soils (Fig. S3, Table S4). With the decrease of particle size, the contents of Al_2O_3, CaO, and $Mg^{\#}$ gradually increase, while the contents of FeO and TiO_2 decrease.

4. Discussion

4.1. Abundance and composition of exotic non-mare components in the CE-6 fine-grained lunar soil

Previous studies have demonstrated that the <45 μm size fractions constitute over 75 % of the surface area of the lunar soil and most closely reflect the bulk lunar soil properties in terms of chemical composition and spectral signature (Cao et al., 2022; Fischer, 1995; Lucey, 2006;

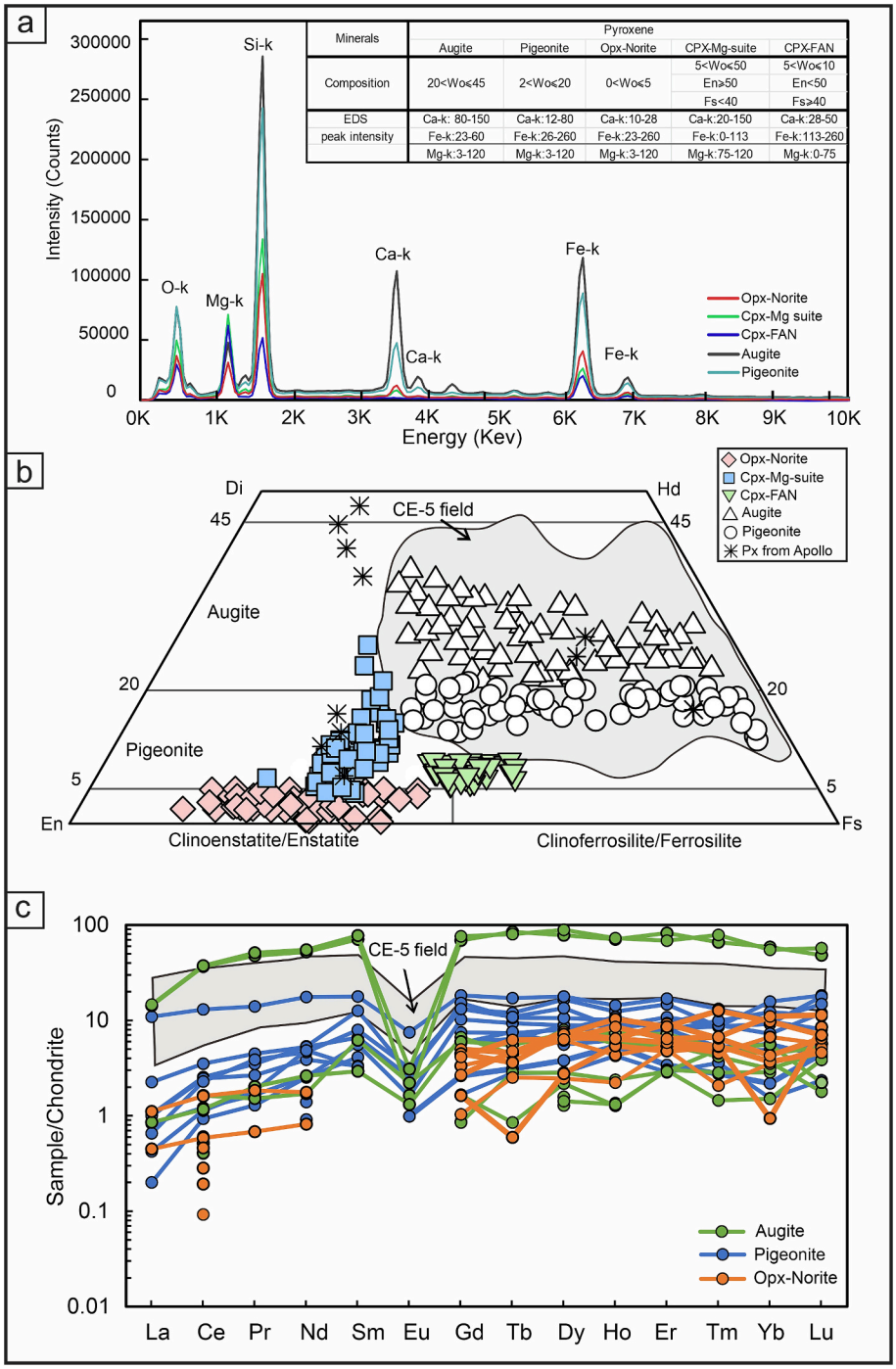

Fig. 3. (a) The EDS spectrum, compositions, and corresponding elemental signal peak intensities used for pyroxene classification in the TIMA system for the CE-6 fine-grained lunar soils. (b) Compositional plot of pyroxenes from lunar highland (ferroan anorthosites and Mg-suite clast) and mare basalt, shown in the "pyroxene quadrilateral." The CE-5 pyroxene fields were sourced from Che et al., 2021; He et al., 2022; Hu et al., 2021; Jiang et al., 2022. The pyroxene data for Apollo basalts are from Papike et al., 1976; Shervais et al., 1990; Vetter et al., 1988. (c) Chondrite-normalized (Anders and Grevesse, 1989) REE patterns of augite, pigeonite and Opx in CE-6 samples. CE-5 pyroxene REE profiles were established based on the data from Tian et al., 2021.

Pieters et al., 1993). These fractions have experienced long-term surface modifications, providing important constraints on the provenance and evolution of lunar soils. The exotic materials from distant and lithologically distinct terrains in lunar samples are crucial to elucidate the magmatic, impact, and weathering characteristics of lunar soil at the landing site (Melosh et al., 2017).

The findings indicate that the fine-grained lunar soil of CE-6 contains at least ~6.5 % exotic non-mare components (Fig. 1k, Fig. S2, Table 1), including pyroxene, plagioclase, and olivine from non-mare units. These three minerals are the most abundant in the lunar crust and mantle rocks, and their compositions vary significantly between rock types. Compared to the compositional variation field of CE-5 pyroxene (Tian et al., 2021, 2023), it revealed that there are three main types of pyroxenes in the exotic non-mare components (Fig. 3a, b, Table 1), namely Mg-rich clinopyroxene, low-Ca pyroxene (pigeonite and orthopyroxene). Among them, orthopyroxene (Opx, 1.2 %) with higher $Mg^{\#}$ generally appears in the norite, Mg-rich clinopyroxene (1.3 %) is more likely from Mg-suite clasts (e.g., troctolite), and low-Ca pigeonite (0.3 %) is the second most abundant mineral in the FAN (Heiken et al., 1991; Li et al., 2024). The pyroxene REE pattern of CE-6 and CE-5 also indicates the presence of pyroxenes from distal terrain in the CE-6 landing site (Fig. 3c, Table S3). The above three pyroxenes from the non-mare have a similar composition to the CE-6 pyroxene analyzed by Shen et al. (2025) and Yin et al. (2025). The An (Ca/(Ca + Na + K)*100, molar percent) of plagioclase varies across different rock types (FAN: ≥95; all types of mare basalt: 72–95 and Mg-suite rocks: 75–98), suggesting that plagioclase fragments in lunar soil can be used to trace the sourced rock types (Cui et al., 2024; Heiken et al., 1991; Papike et al., 1982, 1997; Simon et al., 1982; Wang et al., 2025a; Zhang et al., 2024a). It should be noted that the Chang'e-6 mission collected samples from the regions near the boundary of intermediate-Ti basalt and low-Ti basalt units (interpreted by remote sensing spectral data and corresponding to the 'low-Ti' and 'very low-Ti' in the geochemical data of the CE-6 sample, respectively), and a clast of high-Al basalt from the nearby lunar cryptomaria region has also been identified (Cui et al., 2024; Qian et al., 2024a, 2024b; Zeng et al., 2023; Zhang et al., 2024b). However, very low-Ti or high-Al basalts exhibit mineral compositions that may overlap with those of the Mg-suite (e.g., pyroxene and plagioclase). The broader An value range of 72–90 used in this study includes plagioclase in all types of basalts. The An of plagioclase in exotic non-mare components (0.9 %, Fig. 4a-b) is >95, similar to that of plagioclase from FAN. Additionally, the trace elements (Table S3) of plagioclase also reflect its source (Tian et al., 2023). The early crystallized plagioclase has a higher An content and lower concentrations of incompatible elements (e.g., REE, Sr) (Fig. 4c-d). Olivine is a minor mineral in exotic non-mare components (Fig. 5). Most of the olivine components of mare basalts from the Apollo samples are in the range of Fa 20 (Fig. 5b). The olivine in the exotic non-mare components (0.3 %) has higher $Mg^{\#}$ (>80), representing the composition of dunite and troctolite (Dymek et al., 1975; Marvin and Walker, 1985; Roedder and Weiblen, 1972; Shervais et al., 1985). The study's quantitative statistics on exotic non-mare components in the CE-6 soils will be useful for future research (e.g., in situ isotope analysis, high-precision chronology).

4.2. Implications for the provenance of the CE-6 landing site

The CE-6 landing site lies within the Apollo basin, positioned between two compositional zones of SPA, namely the Mg-pyroxene annulus and the SPA central compositional anomaly, one of the deepest and most geologically significant structures in the SPA basin (Zhang

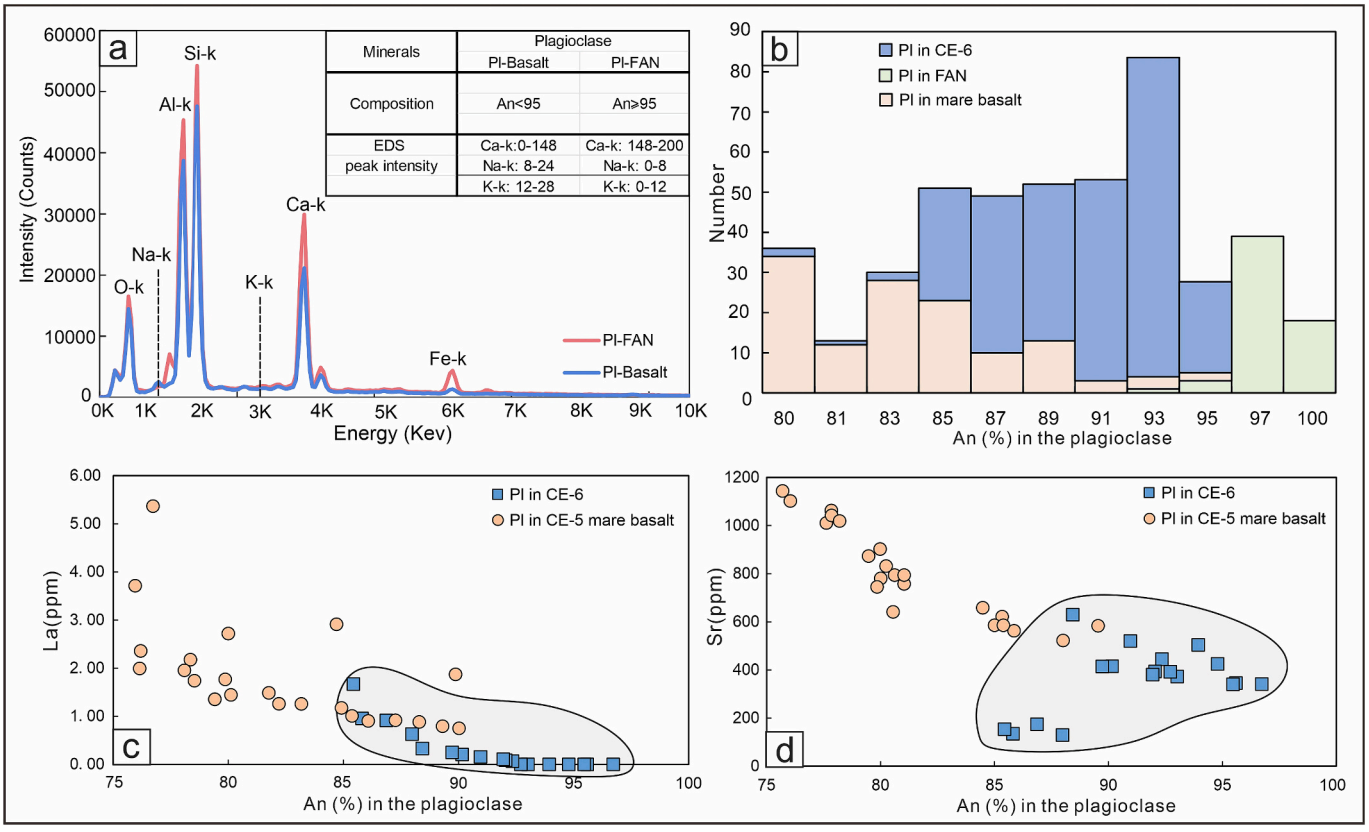

Fig. 4. (a) The EDS spectrum, compositions and corresponding elemental signal peak intensities used for plagioclase classification in the TIMA system for the CE-6 fine-grained lunar soils. (b) Histogram of anorthite component of plagioclase in the CE-6 samples and comparison with those reported from FAN (Roberts et al., 2019; Xu et al., 2020; Zhang et al., 2024a) and mare basalt (He et al., 2022; Li et al., 2023; Tian et al., 2023; Wang et al., 2025a). (c-d) trace elements (c, La; d, Sr) vs. anorthite component of plagioclase in the CE-5 and CE-6, the data in CE-5 mare basalt is from Tian et al., 2021, 2023.

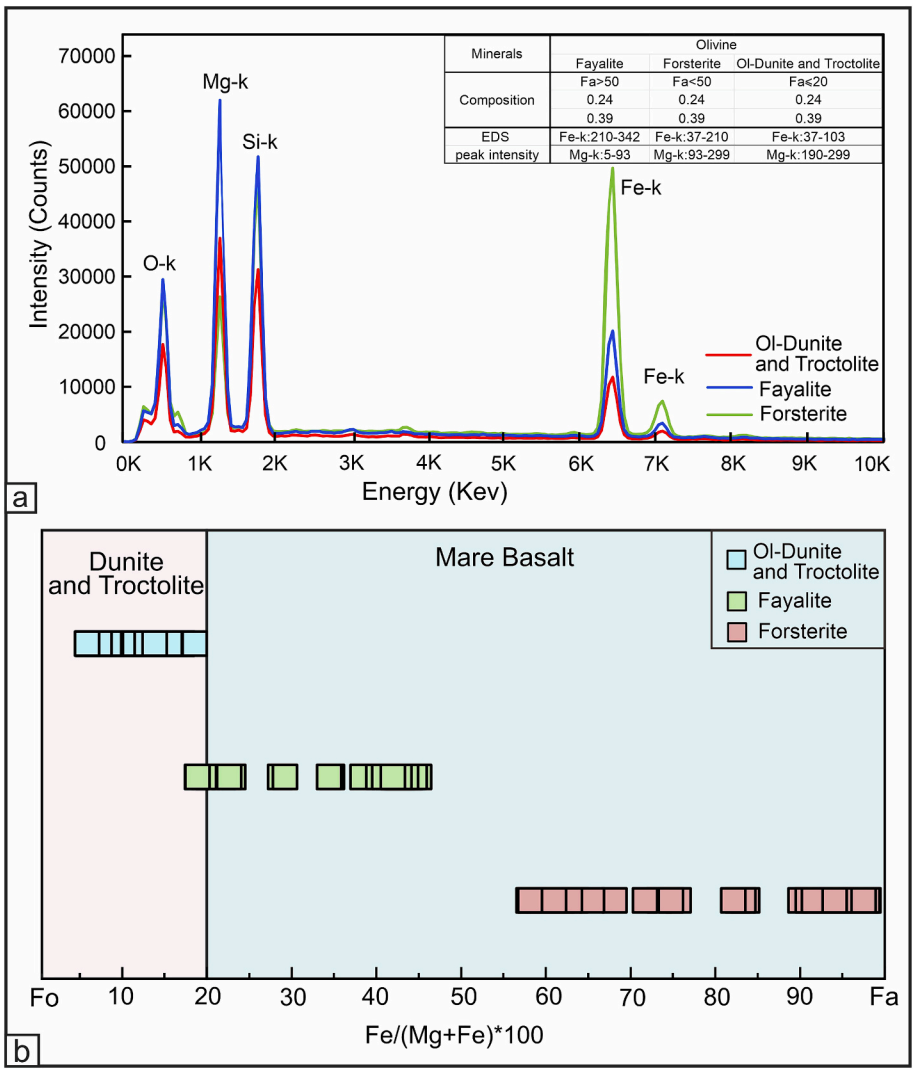

Fig. 5. (a) The EDS spectrum, compositions and corresponding elemental signal peak intensities used for olivine classification in the TIMA system for the CE-6 fine-grained lunar soils. (b) Plots of Fe/(Fe + Mg)*100 variations in olivine from the CE-6 soils. The pink field belongs to the lunar dunite and troctolite, and the blue field is the Mare basalt, which were established based on the data from Dymek et al., 1975; Marvin and Walker, 1985; Roedder and Weiblen, 1972; Shervais et al., 1985. (For interpretation of the references to colour in this figure legend, the reader is referred to the web version of this article.)

et al., 2025). The SPA basin-forming impact, considered the most profound excavation event into the lunar interior, likely displaced upper mantle materials along with extensive impact melt and breccia deposits with a thickness of over tens of kilometers, to the region beneath the CE-6 landing site. These deep-seated materials were subsequently re-excavated by the Apollo basin impact and transported to the CE-6 sampling area, representing a potential source of exotic materials for the CE-6 returned samples (Citron et al., 2024; Melosh et al., 2017; Moriarty and Pieters, 2018; Potter et al., 2018; Yue et al., 2024).

The quantitative analysis revealed that the provenance of CE-6 lunar soil contains a small amount of exotic non-mare components (~6.5 %) (Fig. 1k, Table S2). This finding is consistent with the latest lunar regolith evolution modeling result (Zhang et al., 2025) and suggests the overestimation of some models on exotic materials (Xu et al., 2024). The particle size distribution characteristics indicate that the content of exotic non-mare components has fallen. In contrast, the content of mare basalts rises as the particle size decreases (Fig. 2). The change in soil bulk chemical composition corresponds to the variation in mineral abundance. The reduction of exotic non-mare components reveals the impact gardening processes and exposure time. The impact gardening process is critical in shaping the Moon's surface because it involves repeated overturning, churning, blending, and mixing the top layers of regolith (Melosh, 1991). Su et al. (2024) proposed that the distal ejecta accumulated at the CE-6 landing site, which underwent the impact gardening process at approximately 2.8 Ga. This process will continuously overturn the deep materials onto the lunar surface, mixing and diluting the exotic material that was previously on the surface (Su et al., 2024). Additionally, the impact craters form after the CE-6 basalts (i.e., overlaying on the basalt layer), indicating that the exotic materials have a relatively shorter exposure time and a significantly lower fragmentation than mare basalt. The reasons mentioned above may explain the decrease in abundance of exotic non-mare components with decreasing particle size.

Previous simulation results demonstrate that the minerals in the distal ejecta deposited at the landing site are complex, and each candidate crater has a unique composition (Su et al., 2024; Xu et al., 2024). The first five craters identified around the landing site that could provide the various exotic distal ejecta materials are: Chaffee S ($2.79^{+0.23}_{-0.28}$ Ga, 15.6 cm), Vavilov ($1.86^{+0.12}_{-0.12}$ Ga, 1.7 cm), Crookes (488 Ma, 0.37 cm), Das (719 Ma, 0.5 cm) and Pythagoras ($2.34^{+0.17}_{-0.17}$ Ga, 0.6 cm) (Su et al., 2024; Xu et al., 2024). The modeled ages of these craters are significantly younger or closer to the CE-6 Eratosthenian mare unit ($2.80^{+0.11}_{-0.10}$ Ga). Among them, the Eratosthenian-aged Chaffee S crater, with an

estimated excavation depth of ~1.23 km, based on the 1:10 ratio of excavation depth to transient crater diameter (Melosh, 1991), could transport the largest quantity of exotic materials and is the only decimeter-scale ejecta contributor to CE-6 (Xu et al., 2024). The SPA basin ejecta may have transported the lunar upper mantle material, while the Apollo impact has excavated and redistributed primitive lunar crust material to the surrounding regions (the CE-6 landing site) (Guo et al., 2024; Sun and Lucey, 2024). Recent studies have found Mg-rich orthopyroxenite with high $Mg^{\#}$ (≥85) in the Chaffee S crater, which may represent exposed mantle materials (Sun and Lucey, 2024) or Mg-suite intrusions (Qian et al., 2024a, 2024b). Since the Mg-suite and mantle material could co-exist (Sun and Lucey, 2023), and the original mantle composition may have been diluted during the impact event (Yamamoto et al., 2022), we assume that low-Ca pyroxene in the exotic non-mare components (Opx, 1.2 %) in this study has higher $Mg^{\#}$ (78.1 on average) and negative Eu anomalies (Fig. 3c) that were inherited from their deep source regions in the lunar mantle and excavated by the Chaffee S crater (Qian et al., 2024a, 2024b; Zhang et al., 2025).

Similarly, olivine was identified within the exotic non-mare components (0.3 %, Table 1), with a high average $Mg^{\#}$ of 92.6, consistent with potential mantle dunite composition (Sheng et al., 2025), implying that it originated from olivine-pyroxene mixtures from the Das crater (Karthi, 2019). Plagioclase and pyroxene from FAN (1.2 %, Table 1) are transported to the CE-6 landing site by the Vavilov, Crookes, Das, and Pythagoras craters, which are located in the highlands (Su et al., 2024; Zhang et al., 2025). The different impact craters transport exotic materials of varying composition, increasing the diversity of CE-6 samples. Furthermore, the elevated glass content and higher Al_2O_3, CaO, and $Mg^{\#}$, but lower FeO contents in the bulk composition of CE-6 samples indicate that the CE-6 landing site has undergone a greater impact gardening history than CE-5. The CE-5 sampled young basaltic soils, dominated by locally fragmented and re-cemented materials with little meteorite influence. In contrast, the CE-6 samples have a much longer surface exposure time and have undergone extensive modification, including effects such as impacts, breakage, compaction, and melting, resulting in significantly higher maturity than the CE-5 soils. It has been well established that with a decrease in particle size and an increase in maturity, the composition of lunar soils becomes more feldspathic (Lucey, 2006). The observed shift is attributed not to changes in individual mineral chemistry, but to an increased abundance of plagioclase and glass in smaller grain sizes, as observed by mineral abundance data (Fig. 2). In the <45 μm fraction, these phases are enriched in Al_2O_3, CaO, and MgO, but depleted in FeO and TiO_2. In contrast, minor minerals such as pyroxene and olivine show the opposite trends (Table S2). This mineralogical redistribution explains the bulk-composition differences observed between CE-5 and CE-6 soils. Identifying exotic non-mare components, especially those from mantle materials, is crucial for understanding the Moon's impact history and early evolution.

5. Conclusion

Statistical mineralogy and elemental geochemistry analyses were performed on fine-grained lunar soil returned by CE-6, using automated quantitative mineralogy (TIMA) in conjunction with EPMA and LA-ICPMS. Compared to the CE-5 and CE-6 samples, the fine-grained soils in this study have higher Al_2O_3, CaO, and $Mg^{\#}$ and lower FeO contents. Mineralogical results show that the soils consist of ~93.5 vol% mare basalts and at least ~6.5 vol% exotic non-mare components, and the latter include plagioclase and pigeonite from FAN (0.9 vol%; 0.3 vol%), orthopyroxene from norite (1.2 vol%), pyroxene (1.3 vol%), plagioclase (2.5 vol%) from Mg-suite clast and magnesian olivine from dunite and troctolite fragments (0.3 vol%). Notably, the low-Ca pyroxene and olivine with higher $Mg^{\#}$ values are consistent with ejecta originating from the Chaffee S crater with the mantle composition (e.g., Mg-rich orthopyroxenite, dunite). Additionally, Vavilov, Crookes, Das, and Pythagoras craters in highland regions also provide ejecta materials (e.g., plagioclase and pigeonite from FAN, Cpx from Mg-suite). Analyzing the provenance of the CE-6 landing site through in situ statistical mineral composition is significantly helpful for complementing and verifying the ejecta deposition and regolith growth models.

CRediT authorship contribution statement

Shanna Xue: Writing – review & editing, Writing – original draft, Formal analysis. **Wenlei Song:** Writing – review & editing, Conceptualization. **Zhuang Guo:** Writing – review & editing, Conceptualization. **Yuqi Qian:** Resources. **Kangjun Huang:** Investigation. **Chao Zhang:** Formal analysis. **Qian Liu:** Investigation. **Xiaojun Wang:** Investigation. **Le Qiao:** Formal analysis. **Qian Chen:** Methodology. **Donghai Zhang:** Investigation. **Lihui Chen:** Investigation. **Honglin Yuan:** Methodology, Funding acquisition. **Guochun Zhao:** Project administration.

Declaration of competing interest

The authors declare that they have no known competing financial interests or personal relationships that could have appeared to influence the work reported in this paper.

Acknowledgments

This work was co-supported by grants awarded by the Natural Science Foundation of China (Nos: 42130102, 42273070, 42303039). Y.Q. and G.Z. were funded by the HK RGC grants 17307025, 17308023, and JLFS/P-702/24. We also thank Dr. Marek Dosbaba from TESCAN for improving the TIMA analysis methods.

Appendix A. Supplementary data

Supplementary data to this article can be found online at https://doi.org/10.1016/j.lithos.2025.108265.

References

Anders, E., Grevesse, N., 1989. Abundances of the elements: meteoritic and solar. Geochim. Cosmochim. Acta 53 (1), 197–214.
Beinlich, A., John, T., Vrijmoed, J.C., Tominaga, M., Magna, T., Podladchikov, Y.Y., 2020. Instantaneous rock transformations in the deep crust driven by reactive fluid flow. Nat. Geosci. 13 (4), 307–311.
Breiter, K., Ďurišová, J., Hrstka, T., Korbelová, Z., Vašinová Galiová, M., Müller, A., Simons, B., Shail, R.K., Williamson, B.J., Davies, J.A., 2018. The transition from granite to banded aplite-pegmatite sheet complexes: an example from Megiliggar Rocks, Tregonning topaz granite, Cornwall. Lithos 302–303, 370–388.
Cao, K., Dong, M., She, Z., Xiao, Q., Wang, X., Qian, Y., Li, Y., Wang, Z., He, Q., Wu, X., Zong, K., Hu, Z., Xiao, L., 2022. A novel method for simultaneous analysis of particle size and mineralogy for Chang'E-5 lunar soil with minimum sample consumption. Sci. China Earth Sci. 65 (9), 1704–1714.
Che, X., Nemchin, A., Liu, D., Long, T., Wang, C., Norman, M.D., Joy, K.H., Tartese, R., Head, J., Jolliff, B., Snape, J.F., Neal, C.R., Whitehouse, M.J., Crow, C., Benedix, G., Jourdan, F., Yang, Z., Yang, C., Liu, J., Xie, S., Bao, Z., Fan, R., Li, D., Li, Z., Webb, S. G., 2021. Age and composition of young basalts on the Moon, measured from samples returned by Chang'e-5. Science 374 (6569), 887–890.
Chen, Y., Hu, S., Li, J.-H., Li, Q.-L., Li, X., Li, Y., Liu, Y., Qian, Y., Yang, W., Zhou, Q., Lin, Y., Li, C., Li, X.-H., 2023. Chang'e-5 lunar samples shed new light on the Moon. Innov. Geosci. 1 (1), 100014.
Chen, Q., Song, W., Chen, H., Wang, Z., Guo, Z., Li, Y., Xu, D., Wang, X., Kangjun, H., 2024. Automated fast and quantitative mineralogical characterization of Chang'e-5 lunar soils. At. Spectrosc. 45 (05), 381–390.
Citron, R.I., Smith, D.E., Stewart, S.T., Hood, L.L., Zuber, M.T., 2024. The South Pole-Aitken Basin: Constraints on Impact Excavation, Melt, and Ejecta. Geophys. Res. Lett. 51 (14), e2024GL110034.
Cui, Z., Yang, Q., Zhang, Y.-Q., Wang, C., Xian, H., Chen, Z., Xiao, Z., Qian, Y., Head, J. W., Neal, C.R., Xiao, L., Luo, F., Chen, J., He, P., Cao, Y., Zhou, Q., Huang, F., Chen, L., Wei, B., Wang, J., Yang, Y.-N., Li, S., Yang, Y., Lin, X., Zhu, J., Zhang, L., Xu, Y.-G., 2024. A sample of the Moon's far side retrieved by Chang'e-6 contains 2.83-billion-year-old basalt. Science 386 (6728), 1395–1399.
Ding, C.-L., Nemchin, A., Johnson, T., Norman, M.D., Guan, Y., Tian, L.-L., Xie, W.-L., Li, L.-S., Zhou, S.-D., Xu, K.-X., Wang, X.-L., 2025. A potential mantle origin for precursor rocks of high-Mg impact glass beads in Chang'e-5 soil. Sci. Adv. 11 (19), eadv9019.

Dymek, R.F., Albee, A.L., Chodos, A.A., 1975. Comparative petrology of lunar cumulate rocks of possible primary origin: dunite 72415, troctolite 76535, norite 78235, and anorthosite 62237. Lunar Planet. Sci. Conf. Proc. 1, 301–341.
Fischer, E.M., 1995. Quantitative compositional analysis of the lunar surface from reflectance spectroscopy: iron, aluminum, and model for removing the optical effects of space weathering. Brown University.
Graham, S., Keulen, N., 2019. Nanoscale automated quantitative mineralogy: a 200-nm quantitative mineralogy assessment of fault gouge using mineralogic. Minerals 9 (11), 665.
Guo, D., Bao, Y., Liu, Y., Wu, X., Xu, Y., Yang, Y., Zhang, F., Jolliff, B., Li, S., Zhao, Z., Huang, L., Liu, J., Zou, Y., 2024. Geological investigation of the lunar Apollo basin: from surface composition to interior structure. Earth Planet. Sci. Lett. 646, 118986.
He, Q., Li, Y., Baziotis, I., Qian, Y., Xiao, L., Wang, Z., Zhang, W., Luo, B., Neal, C.R., Day, J.M.D., Pan, F., She, Z., Wu, X., Hu, Z., Zong, K., Wang, L., 2022. Detailed petrogenesis of the unsampled Oceanus Procellarum: the case of the Chang'e-5 mare basalts. Icarus 383, 115082.
Heiken, G.H., Vaniman, D.T., French, B.M., 1991. Lunar Source Book: A User's Guide to the Moon. Cambridge.
Hiesinger, H., Head, J.W., Wolf, U., Jaumann, R., Neukum, G., 2011. Ages and stratigraphy of lunar mare basalts: A synthesis. In: Recent Advances and Current Research Issues in Lunar Stratigraphy. Geol. Soc. Am. Spec. Pap, 447, pp. 1–51.
Hrstka, T., Gottlieb, P., Skála, R., Breiter, K., Motl, D., 2018. Automated mineralogy and petrology - applications of TESCAN Integrated Mineral Analyzer (TIMA). J. Geosci. 63 (1), 47–63.
Hu, S., He, Huicun, Ji, J., Lin, Y., Hui, H., Anand, M., Tartèse, R., Yan, Y., Hao, J., Li, R., Gu, L., Guo, Q., He, Huaiyu, Ouyang, Z., 2021. A dry lunar mantle reservoir for young mare basalts of Chang'e-5. Nature 600 (7887), 49–53.
Jia, B., Fa, W., Zhang, M., Di, K., Xie, M., Tai, Y., Li, Y., 2022. On the provenance of the Chang'E-5 lunar samples. Earth Planet. Sci. Lett. 596, 117791.
Jiang, Y., Li, Y., Liao, S., Yin, Z., Hsu, W., 2022. Mineral chemistry and 3D tomography of a Chang'E 5 high-Ti basalt: implication for the lunar thermal evolution history. Sci. Bull. 67 (7), 755–761.
Karthi, A., 2019. Proc. 50th Lunar and Planetary Science Conference. Lunar and Planetary Institute.
Li, L., Hui, H., Hu, S., Wang, H., Yang, W., Chen, Y., Wu, S., Gu, L., Jia, L., Wu, F., 2023. Petrogenesis of Chang'E-5 young mare low-Ti basalts. Meteorit. Planet. Sci. 58 (10), 1429–1448.
Li, C., Hu, H., Yang, M.-F., Liu, J., Zhou, Q., Ren, X., Liu, B., Liu, D., Zeng, X., Zuo, W., Zhang, G., Zhang, H., Yang, S., Wang, Q., Deng, X., Gao, X., Su, Y., Wen, W., Ouyang, Z., 2024. Nature of the lunar far-side samples returned by the Chang'E-6 mission. Natl. Sci. Rev. 11 (11) nwae328.
Long, T., Qian, Y., Norman, M.D., Miljkovic, K., Crow, C., Head, J.W., Che, X., Tartèse, R., Zellner, N., Yu, X., Xie, S., Whitehouse, M., Joy, K.H., Neal, C.R., Snape, J.F., Zhou, G., Liu, S., Yang, C., Yang, Z., Wang, C., Xiao, L., Liu, D., Nemchin, A., 2022. Constraining the formation and transport of lunar impact glasses using the ages and chemical compositions of Chang'e-5 glass beads. Sci. Adv. 8 (39), eabq2542.
Lucey, P., 2006. Understanding the lunar surface and space-Moon interactions. Rev. Mineral. Geochem. 60 (1), 83–219.
Marvin, U.B., Walker, D., 1985. A transient heating event in the history of a highlands troctolite from Apollo 12 soil 12033. J. Geophys. Res. Solid Earth 90 (S02), C421–C429.
Melosh, H.J., 1991. Impact Cratering: A Geologic Process. Oxford.
Melosh, H.J., Kendall, J., Horgan, B., Johnson, B.C., Bowling, T., Lucey, P.G., Taylor, G. J., 2017. South Pole–Aitken basin ejecta reveal the Moon's upper mantle. Geology 45 (12), 1063–1066.
Moriarty, D.P., Pieters, C.M., 2018. The character of South Pole-Aitken basin: patterns of surface and subsurface composition. J. Geophys. Res. Planets 123 (3), 729–747.
Papike, J.J., Hodges, F.N., Bence, A.E., Cameron, M., Rhodes, J.M., 1976. Mare basalts: crystal chemistry, mineralogy, and petrology. Rev. Geophys. 14 (4), 475–540.
Papike, J.J., Simon, S.B., Laul, J.C., 1982. The lunar regolith: chemistry, mineralogy, and petrology. Rev. Geophys. 20 (4), 761–826.
Papike, J.J., Fowler, G.W., Shearer, C.K., 1997. Evolution of the lunar crust: SIMS study of plagioclase from ferroan anorthosites. Geochim. Cosmochim. Acta 61 (11), 2343–2350.
Paton, C., Hellstrom, J., Paul, B., Woodhead, J., Hergt, J., 2011. Iolite: freeware for the visualisation and processing of mass spectrometric data. J. Anal. At. Spectrom. 26 (12), 2508.
Pieters, C.M., Fischer, E.M., Rode, O., Basu, A., 1993. Optical effects of space weathering: the role of the finest fraction. J. Geophys. Res. Planets 98 (E11), 20817–20824.
Potter, R.W.K., Head, J.W., Guo, D., Liu, J., Xiao, L., 2018. The Apollo peak-ring impact basin: insights into the structure and evolution of the South Pole–Aitken basin. Icarus 306, 139–149.
Qian, Y., Xiao, L., Head, J.W., Wöhler, C., Bugiolacchi, R., Wilhelm, T., Althoff, S., Ye, B., He, Q., Yuan, Y., Zhao, S., 2021. Copernican-aged (<200 Ma) impact ejecta at the Chang'e-5 landing site: statistical evidence from crater morphology, morphometry, and degradation models. Geophys. Res. Lett. 48 (20), e2021GL095341.
Qian, Y., Head, J., Michalski, J., Gong, S., Yang, W., Wang, Z., Xiao, L., Li, X., Zhao, G., 2024a. Extensive intrusive magmatism in the lunar Farside Apollo and South Pole–Aitken Basins, Chang'e-6 landing site. Astrophys. J. Lett. 971 (2), L39.
Qian, Y., Head, J., Michalski, J., Wang, X., Van Der Bogert, C.H., Hiesinger, H., Sun, L., Yang, W., Xiao, L., Li, X., Zhao, G., 2024b. Long-lasting farside volcanism in the Apollo basin: Chang'e-6 landing site. Earth Planet. Sci. Lett. 637, 118737.
Roberts, S.E., McCanta, M.C., Jean, M.M., Taylor, L.A., 2019. New lunar meteorite NWA 10986: a mingled impact melt breccia from the highlands—a complete cross section of the lunar crust. Meteorit. Planet. Sci. 54 (12), 3018–3035.
Roedder, E., Weiblen, P.W., 1972. Petrographic features and petrologic significance of melt inclusions in Apollo 14 and 15 rocks. Lunar Planet. Sci. Conf. Proc. 3, 251.
Sharpton, V.L., 2014. Outcrops on lunar crater rims: Implications for rim construction mechanisms, ejecta volumes and excavation depths. J. Geophys. Res. Planets 119 (1), 154–168.
Shen, D., Li, Shijie, Li, Shaolin, Xu, Y., Li, Y., Li, M., Wang, D., Pang, R., Zhang, Y., Han, Z., 2025. Petrogenesis of Chang'E-6 basalts and implication for multi-episode volcanism in the lunar farside basin. Earth Planet. Sci. Lett. 659, 119335.
Sheng, S.-Z., Wang, S.-J., Li, Q.-L., Wu, S., Wang, H., Hua, J.-X., Chen, Z., Hao, J.-H., Zhang, B., He, Y., Zhu, J.-M., 2025. Lunar primitive mantle olivine returned by Chang'e-6. Nat. Commun. 16 (1), 3759.
Shervais, J.W., Taylor, L.A., Laul, J.C., Shih, C.-Y., Nyquist, L.E., 1985. Very high potassium (VHK) basalt: complications in mare basalt petrogenesis. J. Geophys. Res. Solid Earth 90 (S01), 3–18.
Shervais, J.W., Vetter, S.K., Linstrom, M.M., 1990. Chemical differences between small subsamples of Apollo 15 olivine-normative basalts. Lunar Planet. Sci. Conf. Proc. 20, 109–126.
Simon, S.B., Papike, J.J., Laul, J.C., 1982. The lunar regolith: comparative studies of the Apollo and Luna sites. Petrology of soils from Apollo 17, Luna 16, 20, and 24. Lunar Planet. Sci. Conf. Proc. 12, 371–388.
Su, Y., Xu, L., Zhu, M.-H., Cui, X.-L., 2024. Composition and provenance of the Chang'e-6 lunar samples: insights from the simulation of the impact gardening process. Astrophys. J. Lett. 976 (2), L30.
Su, B., Chen, Y., Wang, Z., Zhang, D., Chen, H., Gou, S., Yue, Z., Liu, Y., Yuan, J., Tang, G., Guo, S., Li, Q., Lin, Y.-T., Li, X.-H., Wu, F.-Y., 2025. South Pole–Aitken massive impact 4.25 billion years ago revealed by Chang'e-6 samples. Natl. Sci. Rev. 12 (6) nwaf103.
Sun, L., Lucey, P.G., 2023. Searching for mantle dunite candidates around the Imbrium basin among the boulder population using high resolution mineral mapping. Earth Planet. Sci. Lett. 610, 118074.
Sun, L., Lucey, P.G., 2024. Lunar mantle composition and timing of overturn indicated by Mg# and mineralogy distributions across the South Pole-Aitken basin. Earth Planet. Sci. Lett. 643, 118931.
Tian, H.-C., Wang, H., Chen, Y., Yang, W., Zhou, Q., Zhang, C., Lin, H.-L., Huang, C., Wu, S.-T., Jia, L.-H., Xu, L., Zhang, D., Li, X.-G., Chang, R., Yang, Y.-H., Xie, L.-W., Zhang, D.-P., Zhang, G.-L., Yang, S.-H., Wu, F.-Y., 2021. Non-KREEP origin for Chang'e-5 basalts in the Procellarum KREEP Terrane. Nature 600 (7887), 59–63.
Tian, H.-C., Yang, W., Zhang, D., Zhang, H., Jia, L., Wu, S., Lin, Y., Li, X., Wu, F., 2023. Petrogenesis of Chang'E-5 mare basalts: clues from the trace elements in plagioclase. Am. Mineral. 108 (9), 1669–1677.
Vetter, S.K., Shervais, J.W., Lindstrom, M.M., 1988. Petrology and geochemistry of olivine-normative and quartz-normative basalts from regolith breccia 15498: new diversity in Apollo 15 mare basalts. Lunar Planet. Sci. Conf. Proc. 18, 255–271.
Wang, Z., Li, Y., Li, J., Zong, K., She, Z., He, Q., Zhao, J., Zhang, W., Zheng, J., Pan, F., Luo, T., Crnobrnja, K., Chen, X., Xiao, L., Hu, Z., Wu, X., Liu, Y., Moynier, F., 2025a. Chemical compositions of Chang'e-6 lunar soil and substantial addition of noritic crust ejecta from Apollo basin. Geology 53 (7), 557–561.
Wang, B.-W., Zhang, Q.W.L., Delano, J.W., Zhang, D., Yang, M.-H., Ouyang, D., Wu, S.-T., Li, Q.-L., 2025b. Size matters: chemical representativeness of lunar impact-generated glass beads. At. Spectrosc. 46 (02), 131–140.
Xie, M., Xiao, Z., Zhang, X., Xu, A., 2020. The Provenance of regolith at the Chang'e-5 candidate landing region. J. Geophys. Res. Planets 125 (5), e2019JE006112.
Xu, C., Kynický, J., Tao, R., Liu, X., Zhang, L., Pohanka, M., Song, W., Fei, Y., 2017. Recovery of an oxidized majorite inclusion from Earth's deep asthenosphere. Sci. Adv. 3 (4), e1601589.
Xu, C., Kynický, J., Song, W., Tao, R., Lü, Z., Li, Y., Yang, Y., Pohanka, M., Galiova, M.V., Zhang, L., Fei, Y., 2018. Cold deep subduction recorded by remnants of a Paleoproterozoic carbonated slab. Nat. Commun. 9 (1), 2790.
Xu, X., Hui, H., Chen, W., Huang, S., Neal, C.R., Xu, X., 2020. Formation of lunar highlands anorthosites. Earth Planet. Sci. Lett. 536, 116138.
Xu, L., Zhang, X., Qiao, L., Lai, J., 2021. Evaluating the thickness and stratigraphy of ejecta materials at the Chang'e-4 landing site. Astron. J. 162 (1), 29.
Xu, L., Qiao, L., Xie, M., Wang, Y., Zhu, M., Yan, J., 2024. Chronology, local stratigraphy, and foreign ejecta materials at the chang'e-6 landing site: constraints on the provenance of samples returned from the Moon's farside. Geophys. Res. Lett. 51 (24), e2024GL111311.
Yamamoto, S., Ohtake, M., Karouji, Y., Kayama, M., Nagaoka, H., Ishihara, Y., Haruyama, J., 2022. Global distribution and geological context of co-existing occurrences of olivine-rich and plagioclase-rich materials on the lunar surface. J. Geophys. Res. Planets 127 (2), e2021JE007077.
Yang, W., Chen, Y., Wang, H., Tian, H.-C., Hui, H., Xiao, Z., Wu, S.-T., Zhang, D., Zhou, Q., Ma, H.-X., Zhang, C., Hu, S., Li, Q.-L., Lin, Y., Li, X.-H., Wu, F.-Y., 2022. Geochemistry of impact glasses in the Chang'e-5 regolith: constraints on impact melting and the petrogenesis of local basalt. Geochim. Cosmochim. Acta 335, 183–196.
Yin, C., Chen, J., Fu, X., Cao, H., Lu, X., Liu, Y., Li, J., Chi, S., Zeng, X., Ling, Z., 2025. Petrogenesis of Chang'e-6 basalts and implication for the young volcanism on the lunar farside. Astrophys. J. Lett. 981 (1), L2.
Yue, Z., Gou, S., Sun, S., Yang, W., Chen, Y., Wang, Y., Lin, H., Di, K., Lin, Y., Li, X., Wu, F., 2024. Geological context of the Chang'e-6 landing area and implications for sample analysis. The Innovation 5 (5), 100663.
Zeng, X., Li, X., Liu, J., 2022. Exotic clasts in Chang'e-5 regolith indicative of unexplored terrane on the Moon. Nat. Astron. 7 (2), 152–159.
Zeng, X., Liu, D., Chen, Y., Zhou, Q., Ren, X., Zhang, Z., Yan, W., Chen, W., Wang, Q., Deng, X., Hu, H., Liu, J., Zuo, W., Head, J.W., Li, C., 2023. Landing site of the

Chang'e-6 lunar farside sample return mission from the Apollo basin. Nat. Astron. 7 (10), 1188–1197.
Zhang, L., Yang, Y.-N., Chen, Z.-M., Wang, J., Wang, C.-Y., Cui, Z.-X., Zhang, Y.-Q., Xu, Y.-G., 2024a. Elemental and Sr isotopic compositions of plagioclase as an indicator of lunar source-rock type: Insights from Chang'e 5 plagioclase fragments. Icarus 413, 116002.
Zhang, Q.W.L., Yang, M.-H., Li, Q.-L., Liu, Y., Yue, Z.-Y., Zhou, Q., Chen, L.-Y., Ma, H.-X., Yang, S.-H., Tang, X., Zhang, G.-L., Ren, X., Li, X.-H., 2024b. Lunar farside volcanism 2.8 billion years ago from Chang'e-6 basalts. Nature 1–2.
Zhang, M., Fa, W., Jia, B., 2025. Provenance and evolution of lunar regolith at the Chang'e-6 sampling site. Nat. Astron. 9 (6), 813–823.
Zong, K., Wang, Z., Li, J., He, Q., Li, Y., Becker, H., Zhang, W., Hu, Z., He, T., Cao, K., She, Z., Wu, X., Xiao, L., Liu, Y., 2022. Bulk compositions of the Chang'E-5 lunar soil: Insights into chemical homogeneity, exotic addition, and origin of landing site basalts. Geochim. Cosmochim. Acta 335, 284–296.